Experimental Characterization of Commercial and Synthesized Aromatic Polyamide Films for Reverse Osmosis Membranes

Xuefan Song, Wafa Guiga, Bernard Rousseau, Anne Jonquieres, Raphaël Weil, Marion Grzelka, Jehan Waeytens, Alexandre Dazzi, Diana Dragoe, and Claire Fargues*
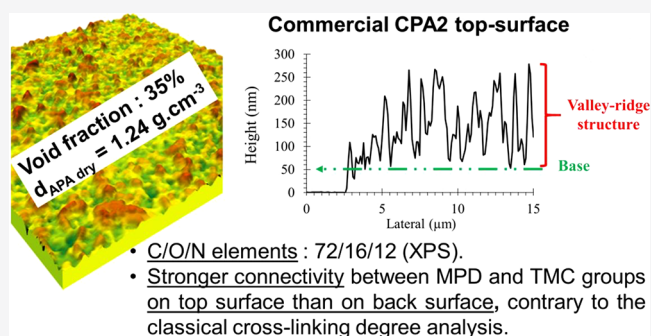
Read Online

ACCESS | Metrics & More | Article Recommendations

ABSTRACT: The complex structure of the active aromatic polyamide (APA) layer of reverse osmosis membranes needs to be precisely described for understanding and predicting solute rejection. A commercial reverse osmosis membrane (CPA2, Hydranautics) was chosen as a case study, and home-made APA films were prepared by free-standing interfacial polymerization of trimesoyl chloride (TMC) and *m*-phenylenediamine (MPD) at different temperatures to obtain different film structures. Their morphology, thickness, void fraction, density, and chemical composition were characterized by scanning electron microscopy (SEM), atomic force microscopy (AFM), profilometry, ellipsometry, dynamic vapor sorption (DVS), and X-ray photoelectron spectroscopy (XPS). All samples have a multilevel topological structure as a dense base upon which generate a valley−ridge structure for CPA2 and a chimneylike structure for synthesized samples, whose thicknesses increase with temperature. An average void fraction of 35% was deduced for the APA from CPA2, allowing the calculation of a dry density of its dense phase of 1.24 g·cm^{-3}, which is rarely investigated for commercial membranes. New chemical descriptors considering chain heads, tails, and branches were introduced to improve the interpretation of chemical composition results. Being more realistic than the cross-linking degree, they suggested for the CPA2 active layer a back surface chemically less cross-linked than the top surface.

Commercial CPA2 top-surface

Void fraction : 35%
$d_{APA\ dry}$ = 1.24 g.cm^{-3}

Valley-ridge structure

Base

- C/O/N elements : 72/16/12 (XPS).
- Stronger connectivity between MPD and TMC groups on top surface than on back surface, contrary to the classical cross-linking degree analysis.

1. INTRODUCTION

Reverse osmosis (RO) is extensively used for pure water production and industrial wastewater treatment in various fields[1−4] due to advantages such as continuity, easy scaling-up, minimum consumption of chemicals, and absence of toxic byproducts.[5,6] Its broad applicability in industrial wastewater treatment includes the removal of trace levels of micropollutants, such as pharmaceutical compounds[7,8] and pesticides.[9,10]

However, the rejection and transfer behavior of small neutral organic components (molecular weight (MW) <180 g·mol^{-1}) remain difficult to predict. Previous studies showed that organic rejection was affected not only by the molecular weight or size but also by specific solute−membrane interactions[11−16] linked to solutes' as well as membranes' chemical properties. For these membranes, the top layer in cross-linked aromatic polyamide (APA, thickness ~200 nm), interfacially polymerized on a microporous polysulfone (PSf) support, dominates membrane selectivity. A solution-diffusion model commonly represents the transfer through it.[17−19] The complex structure of the APA layer needs to be precisely described for understanding and predicting solute rejection. This requires the determination of several key parameters, notably thickness, density, roughness, void fraction,

cross-linking degree, etc.[20,21] Scanning electron microscopy (SEM), transmission electron microscopy (TEM), and atomic force microscopy (AFM) applied on the APA surface and cross section shed light on the thickness, morphology, and roughness information,[22−31] while spectroscopic ellipsometry and a quartz crystal microbalance[23,32−34] may allow access to the void fraction in this layer, crucial to determine accurately the density of the dense APA phase, excluding voids. X-ray photoelectron spectroscopy (XPS),[23,32,35−37] Rutherford backscattering (RBS),[33,38,39] and Fourier transform infrared (FTIR) spectroscopy[26,36] also help in understanding whether the polymerization conditions affect the layer's chemical structure. Indeed, a depth-dependent heterogeneous structure was found,[22,23,38] probably due to *m*-phenylenediamine (MPD) monomer concentration evolution along its diffusion direction during the supported interfacial polymerization. Moreover, Nguyen et al.[40] showed
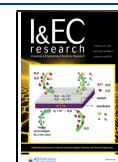
that membranes with different characteristics (thickness, isoelectric point, etc.),[41,42] such as ESPA2 and NF90 membranes, could nevertheless lead to similar performances for glucose, xylose, acetic acid, furfural, or 5-(hydroxymethyl)-furfural (HMF) rejections. A case-to-case study remains therefore essential if a structure–property relationship investigation is intended for a given RO membrane.

In this work, an uncoated and fully aromatic commercial CPA2 RO membrane (Hydranautics, Nitto Group Company), whose rejection performances and sorption properties were extensively studied in our team,[4,12,40,43,44] was chosen as a case study. A better description of the APA structure of commercial membranes is invaluable to improve transfer understanding at the molecular level. To compare its structural properties to those of membranes obtained under constrained conditions, free-standing home-made APA films were synthesized at different temperatures to vary the kinetics and the film structure, as reported by Khorshidi et al.[21] For all samples, morphology and roughness analyses were conducted via SEM, AFM, and profilometry. The thickness was investigated via AFM and profilometry, and spectroscopic ellipsometry was used to search for the void fraction in the APA layer of CPA2, leading to an estimation of two important parameters for the membrane properties, i.e., its effective density as well as that of the dense APA phase. Its chemical composition was also investigated via XPS using new chemical descriptors, which consider chain heads, tails, and branches for going beyond the classical description of cross-linking degree and further improving the structural characterization of these complex APA systems.

2. MATERIALS AND METHODS

2.1. Chemicals. All reagents and chemicals were of analytical grade and used as received: sodium metabisulfite ($Na_2S_2O_5$, Sigma-Aldrich), potassium nitrate (KNO_3, Sigma-Aldrich, ≥99%), ammonium chloride ($NHCl_4$, Sigma-Aldrich, ≥99.5%), sodium bromide (NaBr, VWR Prolabo, 100%), sodium iodide (NaI, Sigma-Aldrich, ≥99%), potassium hydroxide (KOH, Sigma-Aldrich, ≥85%), trimesoyl chloride (TMC, Sigma-Aldrich, 98%), *m*-phenylenediamine (MPD, Sigma-Aldrich, 99%), triethylamine (TEA, Sigma-Aldrich, ≥99%), *N,N*-dimethylformamide (DMF, Sigma-Aldrich, ≥99.9%), chloroform (stabilized with ethanol, Carlo Erba, ≥99%), and *n*-hexane (Carlo Erba, analytical grade for high-performance liquid chromatography (HPLC)). Ultrapure water was produced in the laboratory using a Milli-Q water system (resistivity >18 MΩ·cm, Millipore).

2.2. APA Layer Preparation. *2.2.1. APA Layer Isolation from Commercial CPA2 RO Membrane.* The CPA2 RO membrane was purchased from Hydranautics (Nitto Group Company) as a spiral wound module in the wet state. Its active layer is made of uncoated and fully aromatic polyamide. Membrane samples were initially cut into A4 coupons, rinsed with pure water, then stabilized with 1% sodium metabisulfite solution, and preserved at 4 °C under vacuum. Before using it, the membrane was rinsed with KOH at 0.4 g·L⁻¹ and then with ultrapure water until reaching neutral pH. The polyester layer was peeled off, leading to the ensemble PSf + APA, from which APA was isolated.

The back surface, named as "CPA2-bs," was obtained following the methodology developed by Freger[45] and extensively used since then. Few changes were made to this original methodology: chloroform was first used instead of DMF (more harmful) to dissolve PSf. Then, only a few droplets of

DMF completed the removal of PSf, allowing the APA layer to swell and soften and preventing its deformation such as folding before recovery. Then, the layer stayed flat on the wafer.[45] Dissolution was considered finished when the layer remained completely transparent after solvent evaporation.

To obtain the APA top surface, named as "CPA2-ts," the PSf + APA coupon was immersed in the DMF solvent with the help of a clip fixing the two opposite sides of the coupon with the APA surface facing up. The PSf was completely dissolved in a progressively renewed DMF bath. Only a trace of PSf remained in the solvent at the end according to XPS analysis. The obtained APA film was recovered by introducing underneath a silicon wafer of 1×1 cm^2 and then taken out from the liquid. The APA + wafer ensemble was air-dried and then preserved at 4 °C out of direct light for future analyses.

2.2.2. APA Layer Synthesis. The free-standing aromatic polyamide film samples were synthesized via interfacial polymerization from TMC and MPD following precedent methodologies.[20,46−48] The monomer concentrations and the organic solvent (*n*-hexane) used were typical for the TMC/MPD systems.[20,48,49] The volume of the aqueous phase was the same as that reported by Cui et al.,[46] and the volume of the organic phase was adapted to the Petri dish size to ensure good coverage of the aqueous phase by the TMC organic solution. MPD aqueous solution (20 mL, 3% w/v) containing 1% w/v TEA was poured into a Petri dish (diameter 8.5 cm). Then, 10 mL of TMC (1% w/v) *n*-hexane organic solution was added delicately upon the aqueous surface with the help of a glass plate (size, 2 cm × 5.5 cm) to avoid eddies. The Petri dish was then covered with a glass plate to limit solvent evaporation during interfacial polymerization. A 15 min contact time was necessary to obtain enough APA quantity. Such a reaction time is consistent with other authors.[20,32,47,48] A continuous film was obtained at the interface and the polymerization reaction was stopped: the upper organic solution and lower aqueous phase were removed, while a 2 mm depth of the aqueous phase was maintained to avoid the film adhesion to the Petri dish bottom. Then, the top surface was rinsed three times with 20 mL of *n*-hexane and the back surface was rinsed three times with 20 mL of ultrapure water, always keeping a thin layer of water at the end of each washing step to let the synthesized film float on its surface. The interfacial polymerizations were carried out at three temperatures (−20, cryostat; 0, ice bath; and 29 °C, ambient temperature). Initial aqueous and organic solutions were maintained as close as possible to the target temperature. For the synthesis at −20 °C, the aqueous solution temperature was maintained at around 0 °C to avoid freezing of the aqueous phase. The synthesized samples were labeled in the form of "Syn" + "synthesis temperature" as Syn −20 °C, Syn 0 °C, and Syn 29 °C.

For SEM, AFM, profilometry, and XPS characterizations, the CPA2 and synthesized film samples were all prepared on a silicon wafer of around 1×1 cm^2, and the analyses were realized far from the edges where the film may be folded or damaged, impacting the thickness and chemical composition.

2.3. Structural Characterizations. *2.3.1. Morphology and Thickness Analysis: Field-Emission Scanning Electron Microscopy (FE-SEM), Atomic Force Microscopy (AFM), and Profilometry.* FE-SEM and AFM analyses were performed on APA top and back surfaces of all dry samples.

- FE-SEM (Zeiss SUPRA55-VP) was used with two secondary electron detectors, an in-lens and an Ever-

hart-Thornley SE detector. Samples were mounted onto the steel mesh without usual sputter-coating and then put under vacuum for analysis. The analysis was performed under 1.5 kV to reduce the charging effect, at a magnification of 4000. SmartSEM software was used for data acquisition.

- AFM analyses were performed with a nanoIR2 system (Bruker Nano) to obtain the height profile (or peak-to-valley distance) of the samples placed on a silicon wafer and to study the thickness, morphology, and roughness. The measures were performed in the contact mode, with a gold-coated tip (30 nm diameter) (HQ: CSC38/CR-AU, MicroMasch) and a constant force of around 20 nN. Data acquisition was realized with software Analysis Studio (version 3.15, Bruker Nano), and the images and data were treated with Analysis Studio and MountainsMap (version 8, Digital Surf, France).

For thickness (δ_{AFM}) measurements, frame leveling was realized via MountainsMap's "Series of profile" analysis, which adjusted the cross-sectional height profile of the blank wafer on the horizontal level, line by line. Each point height in the X, Y plane was defined as $Z_{ij} = Z(X_i, Y_j)$. With N_x and N_y as the number of points in X, Y dimensions of a target area, the average height of the area is calculated as

$$\mu = \frac{1}{N_x \cdot N_y} \sum_{j=1}^{N_y} \sum_{i=1}^{N_x} Z_{ij} \tag{1}$$

The heights of the blank wafer (μ_{wafer}) and film region (μ_{film}) on avoiding the edge (the film region within at least 2 μm distance is not analyzed) were calculated independently, and the difference between them was defined as the average film thickness measured by AFM ($\delta_{AFM} = \mu_{film} - \mu_{wafer}$). Besides, the morphology (peak-to-valley distance distribution or height histogram) was analyzed on a detection region of the film of around 10×10 μm^2 area. The statistic roughness was quantified from ten repetitions of 5×5 μm^2 selections and calculated as

$$S_q = \sqrt{\frac{1}{N_x \cdot N_y} \sum_{j=1}^{N_y} \sum_{i=1}^{N_x} (Z_{ij} - \mu)^2} \tag{2}$$

S_q uncertainty was evaluated by the confidence interval at 95% confidence on the ten repetitions.

Cross-sectional profiles of all top surfaces were also extracted from AFM analyses of a 10×30 or 30×30 μm^2 surface of a half-film-covered region on the silicon wafer. The height was recorded along at least 16 different lines. An evaluation of the base thickness (δ_{base}) upon which roughness or irregularities develop was estimated as the lowest level of the valleys detected by the AFM tip and averaged for the different lines analyzed per sample. For CPA2, its back surface was also analyzed.

- Profilometry (DektakXT, Bruker, Germany) was applied to investigate the APA film thickness of CPA2-ts, CPA2-bs, and synthesized samples' top surface. The influence of the relative humidity (RH) on the film thickness (δ_{Pro}) was investigated. Each sample was placed in 95, 79, 59, 40, and 9% RHs at 20 °C using oversaturated salt solutions of potassium nitrate, ammonium chloride, sodium bromide, sodium iodide, or potassium hydroxide, respectively.[50] An incubation time of 7 days ensured the water sorption equilibrium. Just before analysis, the sample was taken out from the conditioned environment onto the profilometry

device in a chamber at ambient humidity (absence of RH control during analysis time). For each sample, between 4 and 10 lines were analyzed with a total analysis duration of less than 10 min. However, between the first and the last analyzed line, no evident thickness evolution was observed, thanks to the short analysis time. S_q analysis of profilometry was only performed at 9% RH.

The analyses were realized with a force of 1 mg and a tip diameter of 4 μm. Data acquisition and treatment were performed via Bruker Vision64 Map software. In this study, data were saved with a spatial resolution of 0.11 μm, except for the sample conditioned at 95% relative humidity (RH), where the resolution was 1.11 μm. The vertical height profile of a straight line around 2 mm long, crossing half-wafer and half-sample region, was analyzed, on which 100 or 200 μm regular and flat regions of sample and silicon wafer profile were selected. As for AFM, δ_{Pro} was calculated as the difference between the average sample and wafer heights of the selected region. Thickness and roughness (S_q) uncertainties were evaluated by a 95% confidence interval for at least four lines.

2.3.2. Void Fraction Estimation by Spectroscopic Ellipsometry Analysis. Spectroscopic ellipsometry (Accurion EP3) was used to determine the refractive index (n_{film}) of the APA layer and deduce its void fraction. The analysis was carried out on dry samples (2% (w/w) water content) obtained after conditioning at 9% RH for 7 days. The sample was taken out from the conditioned environment onto the ellipsometry device before each analysis. Each analysis was launched immediately at ambient humidity and lasted for less than 10 min. Since the water sorption or desorption kinetics was rather slow and corresponded to a low weight gain or loss (3%, w/w) in 10 min, it was considered that the presence of low water content did not interfere with the exploitation of the ellipsometry results. Duplicate samples on silicon wafers were prepared, and at least four locations were analyzed on each. Data acquisition was performed via software EP3View V235, and data modeling was via EP4Model 1.01.

Ellipsometry measures changes in light beam polarization upon specular reflection of the sample, as the ratio of the reflectivity of polarized light in plane (r_p) and out of plane (r_s). The light focusing optics allow adjusting the polarization and offer an optimum condition for the analysis. A multilayer optical model is used to obtain the refractive index of the material by fitting reflectivity ratio (r_p/r_s) with respect to the angle of incidence (AOI, degrees) and wavelength of analysis (λ, nm). Silicon wafer was modeled as a 2 nm silicon dioxide layer (that had been measured independently) and an infinite silicon bottom layer. Each optical layer was described by its thickness (δ), absorption index (k), and refractive index (n). Two AOI values were used (60 and 70°), and the laser beam wavelength was 658 nm. Optical properties for middle and bottom layers were taken as $n = 1.456$, $k = 0$ and $n = 3.829$, $k = 0.014$, respectively. For the APA layer, its thickness was preset as the previously obtained δ_{AFM} or δ_{Pro}, and only n_{film} was fitted assuming $k_{APA} = 0$. The model fitting was accepted when the root-mean-square error (RMSE) was smaller than 100.

According to effective-medium approximation (EMA) models, the void fraction (f_{void}) of the APA film was deduced based on the obtained effective refractive index (n_{film}), the pure dense APA polymer refractive index ($n_{polymer} = n_{APA}$), and that of the void ($n_{void} = n_{air} = 1$), by applying the following models:
Parallel model:

$$n_{\text{film}} = (1 - f_{\text{void}})n_{\text{polymer}} + f_{\text{void}}n_{\text{void}} \qquad (3)$$

Series model:

$$\frac{1}{n_{\text{film}}} = \frac{1 - f_{\text{void}}}{n_{\text{polymer}}} + \frac{f_{\text{void}}}{n_{\text{void}}} \qquad (4)$$

Bruggeman model:

$$1 - f_{\text{void}} = \frac{\frac{n_{\text{film}}^2}{n_{\text{polymer}}^2} - \frac{n_{\text{void}}^2}{n_{\text{polymer}}^2}}{\left(\frac{n_{\text{film}}^2}{n_{\text{polymer}}^2}\right)^{1/3}\left(1 - \frac{n_{\text{void}}^2}{n_{\text{polymer}}^2}\right)} \qquad (5)$$

The choice for a pure dense APA polymer refractive index (n_{polymer}) is discussed in Section 3. Uncertainty on f_{void} was estimated by the average variation between the average value and maximum or minimum ones, issued from the error on n_{film} analysis.

2.3.3. Density Estimation. Samples' mass and their water uptake were measured by a dynamic vapor sorption (DVS) device (Intrinsic Instrument). To obtain a sufficient mass, enough polymer films had to be gathered softly into a pellet, which corresponds to several hundreds of square centimeters due to the extreme thinness of the film.

For APA from CPA2, several dissected films with accurate known surface were progressively gathered in a glass vial, then generously rinsed with ultrapure water via filtration on a nylon filter, and recovered gently together as a pellet with the help of a plastic tweezer. For the home-made APA films, each of them was prepared in a Petri dish (diameter, 8.5 cm), as described in Section 2.2.2. The floating entire surface was recovered from the rinsing water and gathered together softly as a pellet.

The samples were first conditioned in the dry state and then transferred into the DVS device to measure precise masses at controlled RH % (systematic fluctuation of $\pm 0.5\%$). RH levels of 0 and 95% were used to search for the dry and hydrated densities. For each RH stage, the equilibrium time was set as 24 h for CPA2 samples and 48 h for synthesized ones. The dry mass of the samples was between 2.4 and 9 mg.

Considering the heterogeneity of the APA films, three density concepts were investigated to get a more complete understanding of the film structure and dense APA polymer property. The mass of the material (m, g) and film surface (S, cm^2) of thickness δ (cm) lead to

- the areal density

$$d_{\text{areal}} = \frac{m}{S} \ (\text{g·cm}^{-2}) \qquad (6)$$

- the effective volumetric density of the film, which includes voids

$$d_{\text{film}} = \frac{d_{\text{areal}}}{\delta} \ (\text{g·cm}^{-3}) \qquad (7)$$

- the volumetric density of the dense APA region (excluding voids), or referring to the void-free dense phase

$$d_{\text{APA}} = \frac{d_{\text{film}}}{(1 - f_{\text{void}})} \ (\text{g·cm}^{-3}) \qquad (8)$$

For CPA2, the total surface (S) corresponding to the obtained film mass (m) was measured precisely by the ruler before the dissection. For the synthesized films, since they were considered fully recovered after the synthesis, the considered surface S was taken as the total known surface of the Petri dish.

Uncertainties were estimated by the variation between the average and the maximum or minimum values.

2.3.4. X-ray Photoelectron Spectroscopy. The chemical compositions of the CPA2 original top surface and CPA2-bs and CPA2-ts samples were obtained by a ThermoFisher Scientific K-Alpha XPS spectrometer equipped with a monochromatic aluminum source (Al Kα, $h\nu$ = 1486.68 eV) under ultrahigh vacuum conditions (10^{-7} Pa). Samples were previously rinsed thoroughly with ultrapure water and air-dried. The emission angle was set to 0° with an analysis depth of up to 10 nm, the X-ray gun was operated at 10 kV, and a charge neutralization system was used. The survey spectrum acquisition was realized with a sweeping range of 0−1350 eV, a pass energy of 100 eV, and an energy step of 1 eV.

For each sample, at least two frames of 1 cm^2 area were studied, and on each frame, at least three irradiated zones of about 1 mm^2 were analyzed, leading to between 6 and 14 studied zones. The elemental percentages were obtained from the photoelectron peak area using Avantage and CasaXPS software after Shirley-type background subtraction and following normalizations of the peak areas with Scofield sensitivity factors. The initial raw data were treated for eliminating the chemical compositions from the impurities. Notably, for samples of CPA2, when a small amount of sulfur from PSf was detected, the associated oxygen and carbon contents were eliminated on the basis of PSf's $(C_{27}O_4SH_{22})_n$ chemical formula. All data were compared and averaged to ensure the sample representativeness.

3. RESULTS AND DISCUSSION

3.1. Morphology. The CPA2 original top surface observed via SEM appears rather "regular"; however, some images highlight the presence of large node zones (Figure 1). The
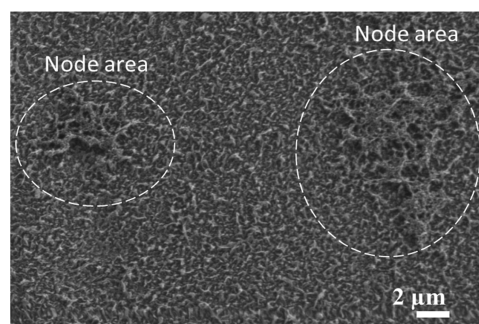

Figure 1. SEM image of the CPA2 original APA top surface.

selection of a representative region is crucial for further analyses; hence, only "regular" regions were selected and compared. Whatever the sample, SEM and AFM methods lead to similar images, while AFM provides a higher resolution (Figure 2). The CPA2 top surface exhibits a typical valley−ridge aspect, already reported for other commercial RO membranes,[51] among which ESPA2 and ESPA3 are from the same supplier.[24,25,27,52] Furthermore, Figure 2 shows that dissection did not damage the APA structure as dissected CPA2-ts is quite similar to the original one. CPA2-bs has a smoother appearance, already noticed for other commercial membranes and explained by the PSf support layer that would prevent the APA's free growth on
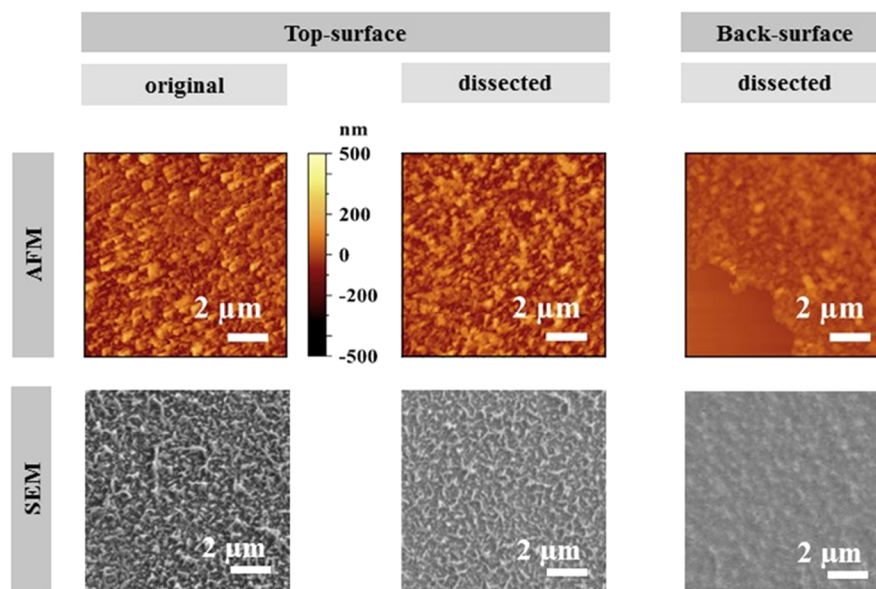
Figure 2. AFM and SEM images of CPA2 APA layers.
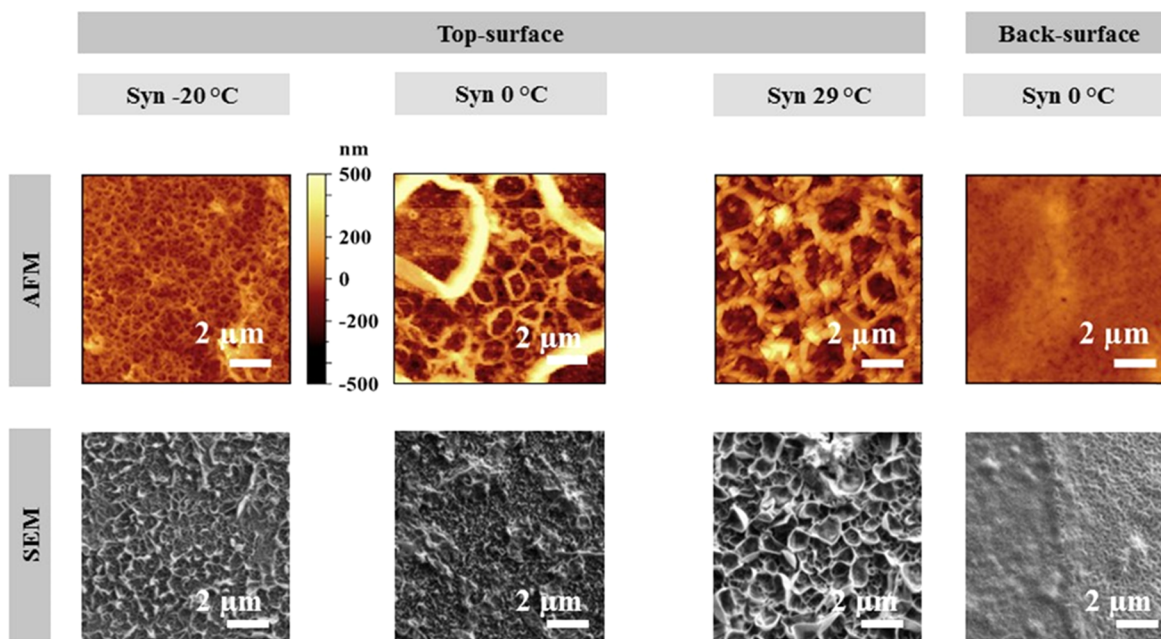

Figure 3. AFM and SEM images of synthesized APA films' top surface and back surface.

that side, as well as by the fact that TMC in the organic upper phase is insoluble in the bottom aqueous phase.[24,25,53]

The morphology of the free-standing synthesized films is significantly different, presenting hollow cylindrical walls forming open inner cavities, which were referred to as "chimneylike structures" or "chimneys" in this study (Figure 3). Even the back surface, although smoother, appears pitted rather than rough. This smooth back surface morphology would again illustrate the polymerization limitation toward the bottom aqueous phase.

While the temperature increase does not influence the back surface aspect, it affects the chimney size on the top surface. AFM reveals a "two-level" or "two-time" polymerization phenomenon at 0 °C, with a base covered by middle-sized chimneys (ranging between the sizes observed at −20 and 29 °C), covered in few places by "top"-chimneys of larger size.

Similar "multilevel" structures have already been observed for free-standing films at the highest reactant concentrations (MPD concentration from 3 to 4%,[37,46] comparable to 3% here) as well as for supported APA films.[32] These authors also reported what they called a general "crumpling phenomenon", magnified by increasing reactant concentrations, especially TMC.[46] In the present work, the chimneys' size increases with temperature (except for the top chimneys solely observed at 0 °C). This observation is consistent with Khorshidi's[21] comment on the influence of synthesis temperature, which would increase the reaction speed and the size of surface features. Furthermore, the polymerization reaction would modify the local temperature, and the resulting thermal gradient consequently leads to Rayleigh−Bénard convection and the creation of local structures,[32] like the chimneys observed in this work. A complementary explanation could be the rapid dissolution of

MPD into the organic phase at the beginning of the free-standing film synthesis, especially due to the high MPD concentration used in the present study. A dense base would then be polymerized at the interface containing enough monomers, while along the diffusion direction (toward the upper organic phase), the MPD concentration would decline progressively,[22,54] leading to coverage by small chimneys. The appearance of large "top" chimneys and formation of a relatively thicker base at 0 °C remained unexplained and could be due to the difficulty in controlling the free-standing polyamide synthesis.

3.2. Thickness, Roughness, and Structure Size. The analysis of the profilometry profiles and AFM images of each sample led to an estimation of the thickness (δ) and roughness (S_q). Thanks to its thinner tip (30 nm compared to 4 μm for the profilometry one), AFM is supposed to fit more precisely the smallest irregularities and thus to describe more accurately the sample roughness. AFM profiles provided

- an estimation of the base thickness (δ_{base}), on which the irregularities develop; and
- the typical size of these irregularities, i.e., the width of a peak (for CPA2 samples) or the diameter and the wall thickness of a chimney (for synthesized samples).

Similar to active layers of other uncoated RO membranes,[23,45,55] no significant swelling was found with RH for CPA2 analyzed by profilometry (Figure 4) neither for
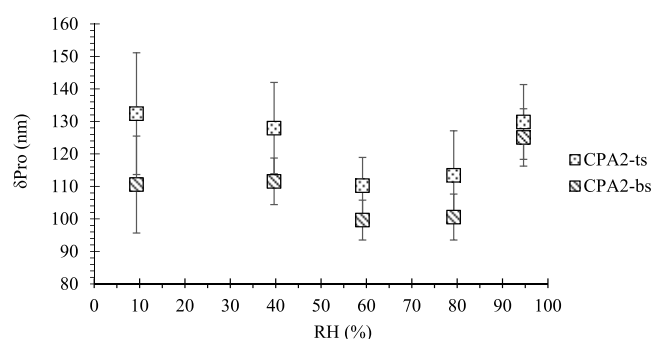
Figure 4. Influence of relative humidity on thickness measured by profilometry for the CPA2 samples.

synthesized samples. This was attributed to the rigidity of these highly cross-linked fully aromatic polyamides. For CPA2, back surface analysis by profilometry leads to a somewhat smaller thickness (δ_{Pro-bs} = 109 nm) than that for top surface (δ_{Pro-ts} = 121 nm) (Table 1), probably due to certain compression of the peaks against the wafer surface. However, the difference between both results is within the uncertainty range. The S_q analysis showed no significant roughness variation

for both surfaces either; hence, it was decided to average APA thickness for CPA2 by profilometry as δ_{Pro} = 115 nm ($\pm$4 nm) and its roughness as S_{q-pro} = 9 nm ($\pm$1 nm).

With AFM, the gap widens between top and back surface thicknesses (δ_{AFM-ts} = 136 nm against δ_{AFM-bs} = 97 nm), probably for the same reason as above. Clearly, the CPA2-ts profile obtained with AFM is much more irregular than that with profilometry (Figure 5). AFM describes more accurately the smallest details of the area explored (Figure 6) and appears more adapted to CPA2-ts roughness measurement, especially with a higher S_{q-ts} = 63 nm ($\pm$2 nm), very close to the XLE's active layer roughness (=64 nm) obtained by the same technique.[33] Moreover, and unlike profilometry, its better sensitivity allows distinguishing back from top surface roughness, with S_{q-bs} = 25 nm ($\pm$1 nm). From Figure 6, a δ_{base} of about 40 nm is obtained, consistent with the literature data for ESPA membranes from the same supplier.[24,52]

For synthesized samples, the thickness tends to increase with synthesis temperature from about 250 nm (at −20 °C) to 450 nm (at 29 °C) (Table 1 and Figures 7 and 8) and allows us to distinguish a "base" thickness, which also seems to increase with temperature. Above this base lies the first level of chimneylike structures whose outer diameter increases with synthesis temperature from 0.5 to 3 μm (Table 1). These elements present thin walls (0.25 μm) and relatively small heights (dozens of nanometers). For the Syn 0 °C sample, a second polymerization level has occurred on top of the first one, as can be deduced from Figure 8c, where a complete cycle wall of a small chimney can be observed under part of one large chimney's wall. These larger chimneys have diameters of around 6 μm, as well as thicker and higher walls (thickness around 1 μm and height up to 700 nm).

3.3. Water Uptake, Void Fraction, and Density Calculation. The water uptake, void fraction (f_{void}), areal density (d_{areal}), film effective volumetric density (d_{film}), and density for dense APA region (d_{APA}) are summarized in Table 2.

Synthesized APA films exhibit important water uptake, up to 65%. Such high values may be related to their high roughness, resulting in a much higher specific area than that of CPA2. It can be noticed that the smaller the chimney diameter (at −20 °C), the higher the specific area and water uptake. The water uptake of APA from CPA2 is around 20%, which is consistent with data reported by Lee et al.[23] for SW30 or by Jiang et al.[37] for synthesized APA film samples (12−22%). The much shorter polymerization time used in the study of Jiang et al.[37] (1 versus 15 min for the present work) may explain the formation of a denser polymer, resulting in a much lower water uptake compared to that of the APA films we synthesized.

The areal density calculated for the synthesized samples appears 4−10 times higher than that of the CPA2 one. The

Table 1. Summary of AFM and Profilometry Characterization of APA Films

		profilometry		AFM		
APA film	$d_{typical}^{a}$ (μm)	δ_{pro} (nm)	S_q (nm)	δ_{AFM} (nm)	δ_{base} (nm)	S_q (nm)
CPA2-ts	0.2−0.5	121 ± 7	10 ± 1	136 ± 1	40	63 ± 2
CPA2-bs	NA	109 ± 5	8 ± 1	97 ± 2	NA	25 ± 1
Syn −20 °C	0.5−1	300 ± 30	180 ± 16	192 ± 2	60	50 ± 8
Syn 0 °C	1−2 and 6[b]	344 ± 25	137 ± 10	396 ± 11	160	176 ± 17
Syn 29 °C	2−3	487 ± 27	149 ± 22	368 ± 15	120	117 ± 5

[a]Width of the ridges for CPA2-ts; chimneylike structure's diameter for synthesized APA samples. [b]For the Syn 0 °C sample, two "levels" of chimneys were obtained.
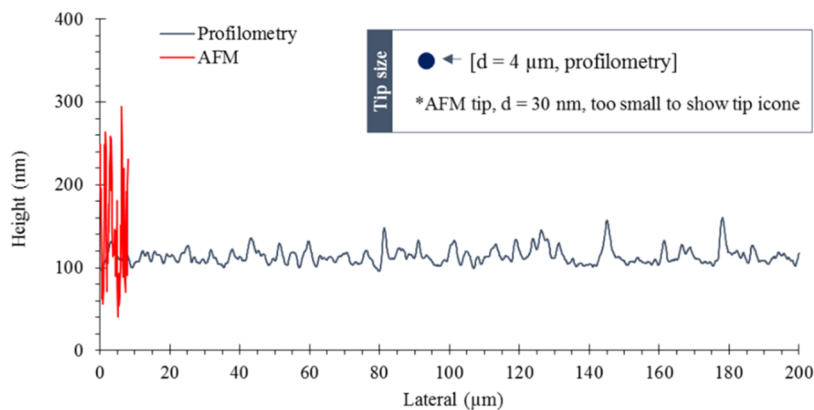
Figure 5. Representative topography profiles of CPA2-ts via profilometry and AFM. Both analyses are realized on distinct sample frames.
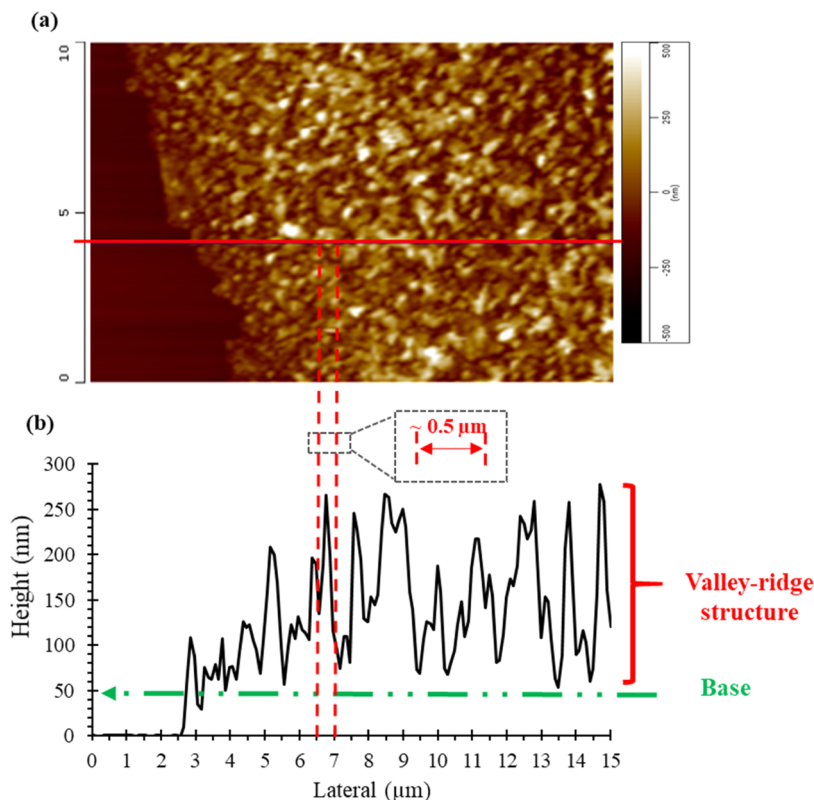

Figure 6. (a) AFM surface images of CPA2-ts and (b) corresponding AFM height profile along the red line. (Analysis of a $10 \times 30 \ \mu m^2$ half-covered sample.).

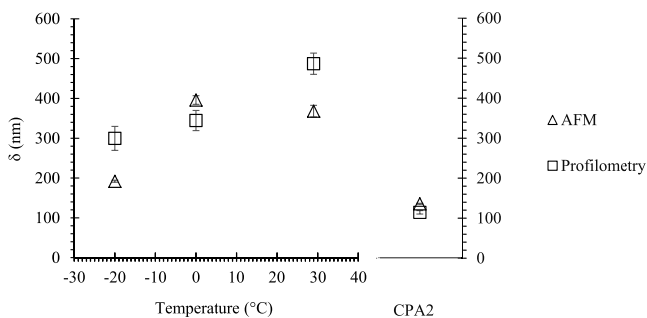**Figure 7.** Top surface thickness analysis via profilometry and AFM for Syn −20 °C, Syn 0 °C, Syn 29 °C, and CPA2 samples.

former should then be 4−10 times thicker compared to CPA2 to obtain a similar effective density d_{film}. This is obviously not the case (Table 1). For the CPA2 APA layer and since no significant swelling took place, thickness values from Table 1 were considered and led to $d_{film} = 0.7 \ g \cdot cm^{-3}$ when dry and $1 \ g \cdot cm^{-3}$ when hydrated. Values obtained for the synthesized samples are much higher and even sometimes unrealistic (up to $3.6 \ g \cdot cm^{-3}$).

Due to their pronounced surface roughness, ellipsometry was found not suitable for analyzing the synthesized samples. Their void fraction and consecutively the density of the dense APA phase therefore could not be determined. A similar difficulty had already been reported by Zhang et al.[56] for FT30 membranes due to their roughness. For the CPA2 sample, using, for example, $\delta_{Pro} = 115$ nm, n_{film} was measured to be 1.40 ± 0.01, which is consistent with the few n_{film} values published for commercial RO
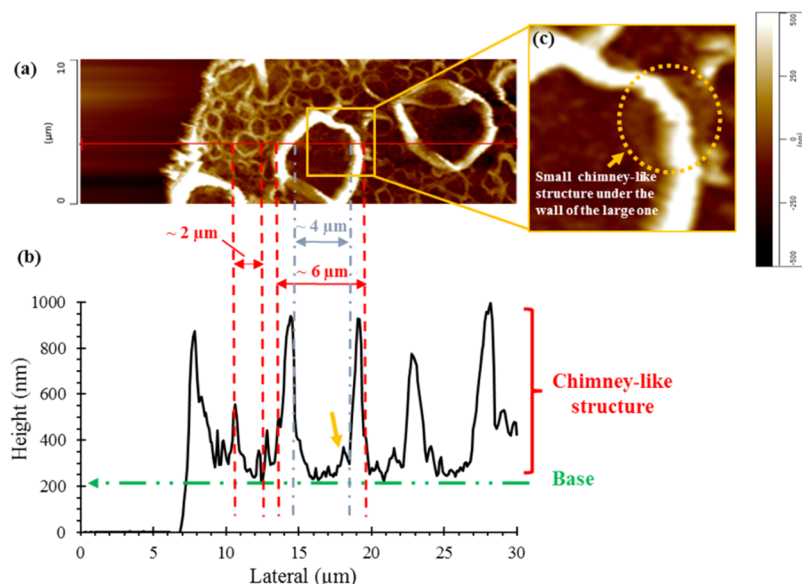
Figure 8. (a) AFM surface images of the Syn 0 °C film, (b) corresponding AFM height profile along the red line, and (c) corresponding enlarged image of the yellow solid box in image (a). (Total analyzed surface = $30 \times 30 \ \mu m^2$.).

Table 2. Density Estimation of the APA Active Layer of CPA2 and the Synthesized APA Films with the Thickness Analyzed with Profilometry and AFM

membrane	f_{void} (%)[a] Pro/AFM	RH (%)[b]	d_{areal} ($\mu g \cdot cm^{-2}$)	water uptake (%, w/w dry basis)	d_{film} ($g \cdot cm^{-3}$)[c] Pro/AFM	d_{APA} ($g \cdot cm^{-3}$) Pro/AFM
CPA2	33 ± 1/38 ± 4	0	10.0 ± 0.5		0.87 ± 0.08/0.74 ± 0.04	1.30 ± 0.14/1.18 ± 0.14
		88	11.9 ± 0.6	19	1.04 ± 0.09/0.88 ± 0.05	1.55 ± 0.16 /1.40 ± 0.17
Syn −20 °C	NA	0	42.1 ± 2.1		1.41 ± 0.21/*2.19 ± 0.13*	NA
		91	69.5 ± 3.5	65	2.32 ± 0.35/*3.62 ± 0.22*	NA
Syn 0 °C	NA	0	67.1 ± 3.4		1.95 ± 0.24/*1.69 ± 0.13*	NA
		92	90.9 ± 4.6	36	2.64 ± 0.33/*2.30 ± 0.18*	NA
Syn 29 °C	NA	0	81.3 ± 4.1		1.67 ± 0.18/*2.21 ± 0.20*	NA
		92	112.0 ± 5.6	38	2.30 ± 0.24/*3.04 ± 0.28*	NA

[a]Estimated from ellipsometry analysis and the series EMA model (with $n_{polymer}$ = 1.74). [b]No swelling took place between 0 and 92% RH. [c]Values in italics are considered as unrealistic

membranes: 1.48 for XLE and 1.43 for ESPA3 active layers.[34] The refractive index of the sample's continuous phase ($n_{polymer}$, here n_{APA}) and that of included air (n_{air}) are required (eqs 3−5) to calculate f_{void}. However, very few values of n_{APA} have been reported previously; hence, three values were tested here: (i) a theoretical estimation at 1.7 based on a group-contribution method[57] used in different studies[11,58] and two estimations via Cauchy model constants on assumed dense nanofilms: (ii) 1.6 calculated from Karan et al.,[32] and (iii) 1.74 from Dennison et al.'s calculation.[39] The resulting CPA2 void fraction appears strongly dependent, at the same time, on this parameter and on the EMA model, with values varying between 23 and 59% (Figure 9). Considering Dennison et al.'s[39] most recent value (n_{APA} = 1.74) and the series EMA model, a void fraction lying between 33% (for δ_{Pro} = 115 nm) and 38% (for δ_{AFM} = 136 nm) was found for the APA film in CPA2, in agreement with the work of Lin et al.,[34] where it was estimated between 21 and 39% for XLE and ESPA3 RO membranes.

Considering an average void fraction of 35% (determined by averaging AFM and profilometry values), a first experimental estimation of d_{APA} for commercial membranes is obtained, about 1.24 $g \cdot cm^{-3}$ when dry and 1.48 $g \cdot cm^{-3}$ when hydrated. The dry value is consistent with the experimental determination made on dense support-free synthesized nanofilms by Dennison et al.[39]
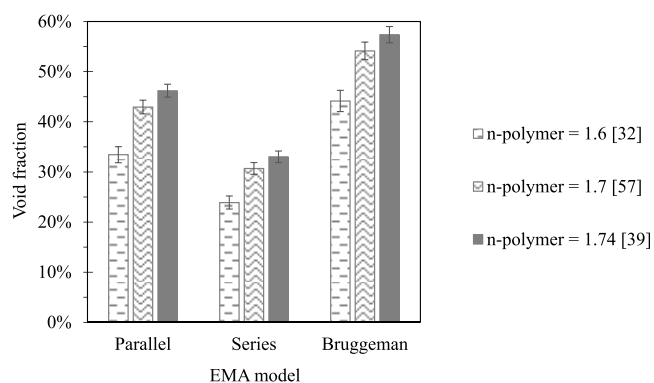
Figure 9. Void fraction estimation via EMA models for the CPA2 APA film for various $n_{polymer}$ data (=n_{APA}) and for δ_{Pro} = 115 nm.

and Karan et al.[32] with the largest densities of 1.26 and 1.44 $g \cdot cm^{-3}$, respectively. Besides, it is in agreement with APA density calculations from molecular modeling studies,[59,60] of around 1.2 $g \cdot cm^{-3}$ for dry samples.

d_{film} values higher than 1.2 $g \cdot cm^{-3}$ while they include voids, as observed for all of the synthesized samples here, seem therefore questionable. Values up to 1.53 $g \cdot cm^{-3}$ were also found for other APA samples from uncoated and fully aromatic commercial
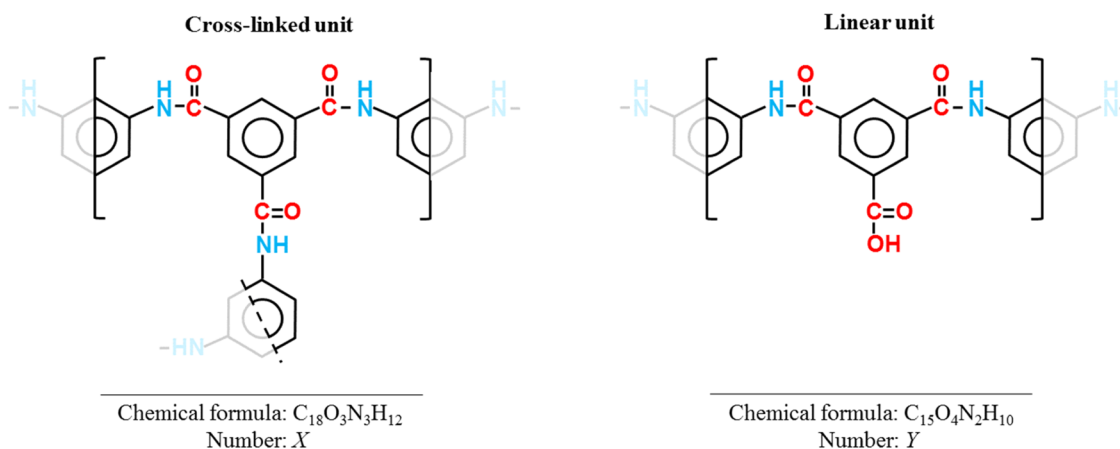
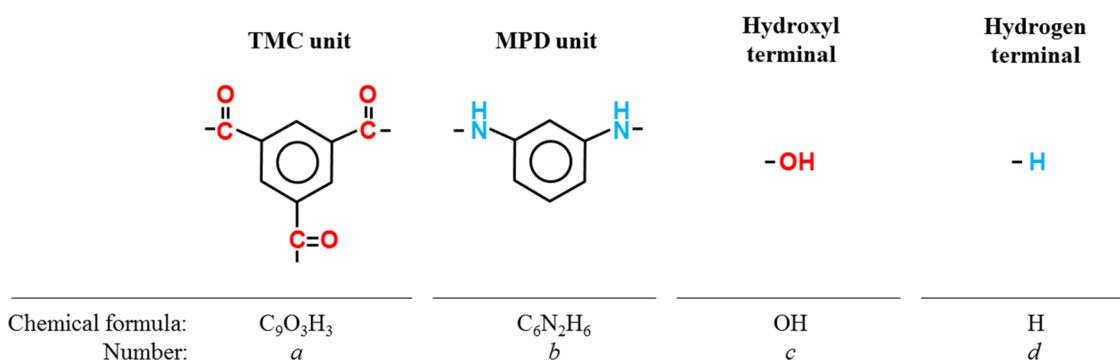**Figure 10.** Chemical units in the conventional scheme for APA.

Figure 11. Chemical units in the new scheme for APA.

membranes.[33] For free-standing synthesized APA dense nano-films, d_{film} values can be deduced from the properties reported in the supporting information of Jiang et al.[37] and generally range from 1.2 to 1.6 $g \cdot cm^{-3}$. Nonetheless, values as high as 2.1 $g \cdot cm^{-3}$ for the rougher films also arise. In all of these cases, excessive densities may be attributed to an underestimation of the APA film thickness, due to its extremely uneven surface.

The above comparative analysis highlights that even sophisticated characterization methods have limitations in this context due to the APA sample's high heterogeneity[22] and very low thickness.[33] They may only shed light on a partial or blurred sample structure.

3.4. Discussion on the Chemical Structure of the CPA2 Membrane. Elemental XPS analyses were used to gain information about the chemical structure of the APA sample from CPA2. Further analyses for synthesized samples still need to be conducted before publication.

3.4.1. From Composition Data to Chemical Structure. In this work, we propose an original approach based on new descriptors for improving the characterization of the APA chemical structure by going beyond the classical cross-linking degree descriptor. The polymer matrix is typically represented as a combination of two chemical units, the cross-linked units X and the linear units Y (Figure 10).

The APA cross-linking degree, χ, is generally expressed as a function of the oxygen to nitrogen ratio, O/N:[21,32,61,62]

$$\chi = \frac{X}{X + Y} = \frac{6}{1 + \frac{O}{N}} - 2 \qquad (9)$$

It assumes that chain heads and tails (TMC or MPD monomers with at least one unreacted amine or acyl group) and branches (short chains connected to the main backbone) have a negligible effect on the chemical composition of the system. A perfect and fully cross-linked APA should then have a repeat unit molecular formula $C_{18}O_3N_3H_{12}$ (unit X, Figure 10) corresponding to an O/N ratio equal to 1 and a carbon fraction (excluding hydrogen atoms, not quantifiable by XPS) equal to 0.75. A fully linear APA will have a repeat unit molecular formula $C_{15}O_4N_2H_{10}$ (unit Y, Figure 10) corresponding to an O/N ratio equal to 2 and a carbon fraction equal to 0.714.

However, the O/N ratio is not a fully distinctive criterion as different structures can be observed with identical O/N ratios. Furthermore, real systems include chain ends and branches such that their composition varies between the limits imposed by the fully linear and fully cross-linked structures. To quantify the relative populations of chain heads, tails, and branches from the XPS analyses, we introduce a new set of four chemical units: a TMC unit, an MPD unit, a hydroxyl terminal unit belonging to an unreacted TMC acid group, and a hydrogen terminal unit belonging to an unreacted MPD amine group. Their number is a, b, c, and d, respectively (Figure 11).

These quantities can be related to the elemental composition using the simple relations $C = 9a + 6b$, $O = 3a + c$, and $N = 2b$. Furthermore, for TMC and MPD backbones, their quantities of amide bond should be equal; hence, we have $2b - d = 3a - c$. The fraction of acyl groups that have reacted, f_{ac}, is given by the number of amide bonds divided by the maximal number of amide bonds that could have been formed for a number a of TMC units:

Table 3. Chemical Composition and Chemical Descriptors of CPA2 Active Layers

CPA2 layer	C %	O %	N %	O/N	χ	f_{ac}	f_{an}	$r_{t:m}$
original top surface	72.1 ± 0.8	17.0 ± 0.9	10.9 ± 0.5	1.56 ± 0.16	0.34 ± 0.14	0.70 ± 0.15	0.84 ± 0.26	0.80 ± 0.08
CPA2-ts	73.1 ± 0.5	15.4 ± 0.4	11.5 ± 0.4	1.34 ± 0.08	0.57 ± 0.08	0.80 ± 0.08	0.90 ± 0.16	0.75 ± 0.06
CPA2-bs	70.3 ± 0.4	15.0 ± 0.4	14.7 ± 0.4	1.02 ± 0.05	0.97 ± 0.08	0.28 ± 0.15	0.16 ± 0.10	0.40 ± 0.03

$$f_{ac} = \frac{3a - c}{3a} = \left(2 - \frac{3O}{C - 3N}\right) \tag{10}$$

The fraction of amine groups that have reacted, f_{am}, is given by the number of amide bonds divided by the maximal number of amide bonds that could have been formed for a number b of MPD units:

$$f_{am} = \frac{2b - d}{2b} = \left(\frac{2C - 3O}{3N} - 2\right) \tag{11}$$

Finally, the TMC/MPD units' ratio, $r_{t:m}$, is simply given by this expression

$$r_{t:m} = \frac{a}{b} = \left(\frac{2C - 6N}{9N}\right) \tag{12}$$

3.4.2. XPS Analysis Data and Chemical Structure of APA Layers. The average C/O/N composition obtained from XPS analysis of CPA2 roughly equals 72/16/12 (Table 3). Within the 95% confidence interval, no definite compositional difference is seen between original and dissected CPA2-ts, showing that the dissection did not modify the membrane chemical structure. On the contrary, a clear difference is observed between top and back surfaces: the top surface is richer in carbon and oxygen elements and poorer in nitrogen element. This difference had already been mentioned in the literature[38] and attributed to the decreasing MPD concentration from the bottom to the top. It impacts the O/N ratio, leading to a much higher cross-linking degree for its back surface ($\chi_{bs} \approx 0.97$) than for its top surface ($\chi_{ts} \approx 0.45$). An opposite conclusion emerges from the evolution of f_{ac}, f_{am}, and $r_{t:m}$, with much lower fractions of connected acyl and amine groups on the back surface, meaning that it would be less "cross-linked" than the top. From back to top surfaces, the TMC/MPD monomeric units' ratio ($r_{t:m}$) increases as a result of the decrease of MPD concentration along the thickness of the membrane,[38] while TMC and MPD become better connected, with less unreacted amine and acyl groups on the top surface. As emphasized by Morgan and Kwolek,[63] during interfacial polymerization, acid chloride group hydrolysis may occur at the interface, where contact with water molecules is possible. This process becomes competitive and consequently alters the cross-linking density.[21] Thus, the lesser connectivity and larger amount of carboxyl groups observed at the back surface could be due to this process.

The possibility of having different chemical structures and compositions across the APA layer thickness has already been suggested by Freger and Srebnik[22,64] and studied in detail recently by Coronell et al.[38] However, there again, opposite conclusions on the cross-linking evolution over thickness arise whether χ or the new descriptors is considered. Indeed, O/N ratios; cross-linking degree χ; and structural descriptors f_{ac}, f_{am}, and $r_{t:m}$ values can be deduced from their chemical composition analyses, run for several RO membranes with XPS experiments for the top surface and Rutherford backscattering spectrometry (RBS) for the volume bulk (Table 4). Larger O/N ratios being measured by XPS than by RBS, the cross-linking degree χ appears lower on top surfaces than in the bulk, as for our CPA2

Table 4. Chemical Structure Descriptor Calculation for APA Active Layers from Coronell et al.[38]

active layer	O/N	χ	f_{ac}	f_{am}	$r_{t:m}$
ESPA3 top surface	1.25	0.66	0.98	1.20	0.82
ESPA3 volume	1.10	0.86	0.71	0.60	0.57
ESPAB top surface	1.46	0.44	0.87	1.13	0.86
ESPAB volume	1.00	1.00	0.86	0.75	0.58
SWC5 top surface	1.10	0.86	1.28	1.94	1.01
SWC5 volume	1.02	0.98	0.86	0.77	0.60
NF90 top surface	1.25	0.66	1.10	1.53	0.93
NF90 volume	1.10	0.85	0.89	0.88	0.66

samples. Meanwhile, structural descriptors f_{ac}, f_{am}, and $r_{t:m}$ lead to an opposite conclusion, as they indicate stronger connectivity between MPD and TMC groups on top surfaces than in the bulk.

This highlights that the cross-linking degree χ, which assumes that no chain ends or defects exist in the polymer structure, must be considered with care and is probably not suitable for the representation of APA in the CPA2 membrane.

4. CONCLUSIONS

The separation and very low thickness of the active layer of commercial RO membranes make its characterization difficult. The CPA2 membrane from Hydranautics was chosen here as a case study, as it had been studied by our team for its rejection of several organic solutes. The structure of its aromatic polyamide layer (APA) can be considered as representative for many other uncoated and fully aromatic reverse osmosis commercial membranes.

As already observed, the top surface of the CPA2 active layer exhibited a typical valley–ridge aspect developed on a base of 40 nm thickness, while its back surface was "flat". Its height was estimated as 115 nm with profilometry and 136 nm with AFM. Thanks to its thinner tip that could investigate more precisely the narrowest and deepest cavities, AFM was found more suitable to evaluate its top surface roughness (63 ± 2 nm). The void fraction in this polymer was found between 33 and 38% through a combination of thickness and ellipsometry analyses, which allowed us to deduce, for the first time to our knowledge, a realistic volumetric density of the sole APA dense polymer of a commercial membrane, about 1.48 g·cm^{-3} when hydrated and 1.24 g·cm^{-3} when dry. The latter value is in good agreement with the few existing data on synthesized APA, as well as with molecular simulation predictions.

XPS analysis of the CPA2 active layer showed a clear compositional difference between top and back surfaces. An original analysis based on new chemical structure descriptors (f_{ac}, f_{am}, and $r_{t:m}$) accounting for chain heads, tails, and branches resulting from nonideal polymerization provided a better insight into its chemical structure, compared to the classical cross-linking degree. A striking result is that different types of descriptors led to opposite conclusions: while the cross-linking degree χ suggested that the CPA2 APA back surface was more cross-linked than the top surface, the new chemical structure

descriptors showed the opposite, with a lower connectivity rate on the back surface than that on the top surface. The cross-linking degree χ was then considered unsuitable to describe this polymer and should be limited to systems with negligible amounts of chain branches, heads, and tails.

To compare different controlled structures, APA films synthesized using free-standing interfacial polymerization at different temperatures were studied. The morphology of their top surface was significantly different from that of the commercial CPA2: AFM allowed us to distinguish a "base" above which developed hollow cylindrical walls or "chimneys", whose size tended to increase with synthesis temperature, as did the average sample thickness, from about 250 nm at −20 °C up to 450 nm at 29 °C. These samples were so uneven that the ellipsometry technique was unsuitable. Consequently, their void fraction and density could not be calculated.

Our study emphasizes that although the density is a very standard property, it remains very difficult to obtain with high accuracy for such complex multilevel structures. An accurate description of their chemical structure such as the cross-linking state appears to be also a challenge in itself, which needs the purest samples and the most precise methods.

■ AUTHOR INFORMATION

Corresponding Author

Claire Fargues − *Université Paris-Saclay, INRAE, AgroParisTech, UMR SayFood, 91300 Massy, France;* orcid.org/0000-0002-2117-1939; Phone: +33 (0)1 69 93 50 95; Email: claire.fargues@agroparistech.fr; Fax: +33 (0) 1 69 93 50 44

Authors

Xuefan Song − *Université Paris-Saclay, INRAE, AgroParisTech, UMR SayFood, 91300 Massy, France; Université Paris-Saclay, CNRS, Institut de Chimie Physique, UMR8000, 91405 Orsay, France*

Wafa Guiga − *Université Paris-Saclay, INRAE, AgroParisTech, UMR SayFood, 91300 Massy, France; Le Cnam, 75005 Paris, France*

Bernard Rousseau − *Université Paris-Saclay, CNRS, Institut de Chimie Physique, UMR8000, 91405 Orsay, France*

Anne Jonquieres − *Laboratoire de Chimie Physique Macromoléculaire (LCPM), UMR 7375, Université de Lorraine, CNRS, LCPM, F-54000 Nancy, France*

Raphaël Weil − *Université Paris-Saclay, CNRS, Laboratoire de Physique des Solides, UMR 8502, 91405 Orsay, France*

Marion Grzelka − *Université Paris-Saclay, CNRS, Laboratoire de Physique des Solides, UMR 8502, 91405 Orsay, France;* orcid.org/0000-0003-0423-662X

Jehan Waeytens − *Université Paris-Saclay, CNRS, Institut de Chimie Physique, UMR8000, 91405 Orsay, France; Structure et Fonction des Membranes Biologiques, Université libre de Bruxelles, 1050 Bruxelles, Belgique;* orcid.org/0000-0003-3964-2986

Alexandre Dazzi − *Université Paris-Saclay, CNRS, Institut de Chimie Physique, UMR8000, 91405 Orsay, France*

Diana Dragoe − *Université Paris-Saclay, CNRS, Institut de Chimie Moléculaire et des Matériaux UMR 8182, 91405 Orsay, France*

Complete contact information is available at:
https://pubs.acs.org/10.1021/acs.iecr.0c05393

Notes

■ REFERENCES

(1) Shenvi, S. S.; Isloor, A. M.; Ismail, A. F. A Review on RO Membrane Technology: Developments and Challenges. *Desalination* **2015**, *368*, 10−26.

(2) Frenzel, I.; Stamatialis, D. F.; Wessling, M. Water Recycling from Mixed Chromic Acid Waste Effluents by Membrane Technology. *Sep. Purif. Technol.* **2006**, *49*, 76−83.

(3) Hoinkis, J.; Panten, V. Wastewater Recycling in Laundries-From Pilot to Large-Scale Plant. *Chem. Eng. Process.* **2008**, *47*, 1159−1164.

(4) Sagne, C.; Fargues, C.; Lewandowski, R.; Lameloise, M. L.; Gavach, M.; Decloux, M. A Pilot Scale Study of Reverse Osmosis for the Purification of Condensate Arising from Distillery Stillage Concentration Plant. *Chem. Eng. Process.* **2010**, *49*, 331−339.

(5) Al-Bastaki, N. M. Performance of Advanced Methods for Treatment of Wastewater: UV/TiO2, RO and UF. *Chem. Eng. Process.* **2004**, *43*, 935−940.

(6) Sonune, A.; Ghate, R. Developments in Wastewater Treatment Methods. *Desalination* **2004**, *167*, 55−63.

(7) Li, C.; Yang, Y.; Liu, Y.; Hou, L. Removal of PhACs and Their Impacts on Membrane Fouling in NF/RO Membrane Filtration of Various Matrices. *J. Membr. Sci.* **2018**, *548*, 439−448.

(8) Licona, K. P. M.; Geaquinto, L. R. d. O.; Nicolini, J. V.; Figueiredo, N. G.; Chiapetta, S. C.; Habert, A. C.; Yokoyama, L. Assessing Potential of Nanofiltration and Reverse Osmosis for Removal of Toxic Pharmaceuticals from Water. *J. Water Process Eng.* **2018**, *25*, 195−204.

(9) Fini, M. N.; Madsen, H. T.; Muff, J. The Effect of Water Matrix, Feed Concentration and Recovery on the Rejection of Pesticides Using NF/RO Membranes in Water Treatment. *Sep. Purif. Technol.* **2019**, *215*, 521−527.

(10) Plakas, K. V.; Karabelas, A. J. Removal of Pesticides from Water by NF and RO Membranes—A Review. *Desalination* **2012**, *287*, 255−265.

(11) Ben-David, A.; Bason, S.; Jopp, J.; Oren, Y.; Freger, V. Partitioning of Organic Solutes between Water and Polyamide Layer of RO and NF Membranes: Correlation to Rejection. *J. Membr. Sci.* **2006**, *281*, 480−490.

(12) Fargues, C.; Sagne, C.; Szymczyk, A.; Fievet, P.; Lameloise, M. L. Adsorption of Small Organic Solutes from Beet Distillery Condensates on Reverse-Osmosis Membranes: Consequences on the Process Performances. *J. Membr. Sci.* **2013**, *446*, 132−144.

(13) Ghoufi, A.; Dražević, E.; Szymczyk, A. Interactions of Organics within Hydrated Selective Layer of Reverse Osmosis Desalination Membrane: A Combined Experimental and Computational Study. *Environ. Sci. Technol.* **2017**, *51*, 2714−2719.

(14) Liu, Y.; Wang, X.; Yang, H.; Xie, Y. F. Quantifying the Influence of Solute-Membrane Interactions on Adsorption and Rejection of Pharmaceuticals by NF/RO Membranes. *J. Membr. Sci.* **2018**, *551*, 37−46.

(15) Nghiem, L. D.; Schäfer, A. I.; Elimelech, M. Removal of Natural Hormones by Nanofiltration Membranes: Measurement, Modeling, and Mechanisms. *Environ. Sci. Technol.* **2004**, *38*, 1888−1896.

(16) Bellona, C.; Drewes, J. E.; Xu, P.; Amy, G. Factors Affecting the Rejection of Organic Solutes during NF/RO Treatment—A Literature Review. *Water Res.* **2004**, *38*, 2795−2809.

(17) Soltanieh, M.; Gill, W. N. Review of Reverse Osmosis Membranes and Transport Models. *Chem. Eng. Commun.* **1981**, *12*, 279−363.

(18) Wijmans, J. G.; Baker, R. W. The Solution-Diffusion Model: A Review. *J. Membr. Sci.* **1995**, *107*, 1−21.

(19) Williams, M. E.; Hestekin, J. A.; Smothers, C. N.; Bhattacharyya, D. Separation of Organic Pollutants by Reverse Osmosis and Nanofiltration Membranes: Mathematical Models and Experimental Verification. *Ind. Eng. Chem. Res.* **1999**, *38*, 3683−3695.

(20) Ettori, A. Vieillissement Chimique de Membranes d'osmose Inverse. Ph.D. Thesis, Université Toulouse III—Paul Sabatier: Toulouse, France, 2011.

(21) Khorshidi, B.; Thundat, T.; Fleck, B. A.; Sadrzadeh, M. A Novel Approach Toward Fabrication of High Performance Thin Film Composite Polyamide Membranes. *Sci. Rep.* **2016**, *6*, No. 22069.

(22) Freger, V. Nanoscale Heterogeneity of Polyamide Membranes Formedby Interfacial Polymerization. *Langmuir* **2003**, *19*, 4791−4797.

(23) Lee, J.; Doherty, C. M.; Hill, A. J.; Kentish, S. E. Water Vapor Sorption and Free Volume in the Aromatic Polyamide Layer of Reverse Osmosis Membranes. *J. Membr. Sci.* **2013**, *425−426*, 217−226.

(24) Yan, H.; Miao, X.; Xu, J.; Pan, G.; Zhang, Y.; Shi, Y.; Guo, M.; Liu, Y. The Porous Structure of the Fully-Aromatic Polyamide Film in Reverse Osmosis Membranes. *J. Membr. Sci.* **2015**, *475*, 504−510.

(25) Pacheco, F.; Sougrat, R.; Reinhard, M.; Leckie, J. O.; Pinnau, I. 3D Visualization of the Internal Nanostructure of Polyamide Thin Films in RO Membranes. *J. Membr. Sci.* **2016**, *501*, 33−44.

(26) Hermans, S.; Bernstein, R.; Volodin, A.; Vankelecom, I. F. J. Study of Synthesis Parameters and Active Layer Morphology of Interfacially Polymerized Polyamide-Polysulfone Membranes. *React. Funct. Polym.* **2015**, *86*, 199−208.

(27) Tang, C. Y.; Kwon, Y.-N.; Leckie, J. O. Probing the Nano- and Micro-Scales of Reverse Osmosis Membranes—A Comprehensive Characterization of Physiochemical Properties of Uncoated and Coated Membranes by XPS, TEM, ATR-FTIR, and Streaming Potential Measurements. *J. Membr. Sci.* **2007**, *287*, 146−156.

(28) Xu, J.; Yan, H.; Zhang, Y.; Pan, G.; Liu, Y. The Morphology of Fully-Aromatic Polyamide Separation Layer and Its Relationship with Separation Performance of TFC Membranes. *J. Membr. Sci.* **2017**, *541*, 174−188.

(29) Song, X.; Gan, B.; Yang, Z.; Tang, C. Y.; Gao, C. Confined Nanobubbles Shape the Surface Roughness Structures of Thin Film Composite Polyamide Desalination Membranes. *J. Membr. Sci.* **2019**, *582*, 342−349.

(30) Song, X.; Gan, B.; Qi, S.; Guo, H.; Tang, C. Y.; Zhou, Y.; Gao, C. Intrinsic Nanoscale Structure of Thin Film Composite Polyamide Membranes: Connectivity, Defects, and Structure–Property Correlation. *Environ. Sci. Technol.* **2020**, *54*, 3559−3569.

(31) Peng, L. E.; Yao, Z.; Yang, Z.; Guo, H.; Tang, C. Y. Dissecting the Role of Substrate on the Morphology and Separation Properties of Thin Film Composite Polyamide Membranes: Seeing Is Believing. *Environ. Sci. Technol.* **2020**, *54*, 6978−6986.

(32) Karan, S.; Jiang, Z.; Livingston, A. G. Sub-10 Nm Polyamide Nanofilms with Ultrafast Solvent Transport for Molecular Separation. *Science.* **2015**, *348*, 1347−1351.

(33) Lin, L.; Feng, C.; Lopez, R.; Coronell, O. Identifying Facile and Accurate Methods to Measure the Thickness of the Active Layers of Thin-Film Composite Membranes—A Comparison of Seven Characterization Techniques. *J. Membr. Sci.* **2016**, *498*, 167−179.

(34) Lin, L.; Lopez, R.; Ramon, G. Z.; Coronell, O. Investigating the Void Structure of the Polyamide Active Layers of Thin-Film Composite Membranes. *J. Membr. Sci.* **2016**, *497*, 365−376.

(35) Khorshidi, B.; Thundat, T.; Fleck, B. A.; Sadrzadeh, M. Thin Film Composite Polyamide Membranes: Parametric Study on the Influence of Synthesis Conditions. *RSC Adv.* **2015**, *5*, 54985−54997.

(36) Tang, C. Y.; Kwon, Y.-N.; Leckie, J. O. Effect of Membrane Chemistry and Coating Layer on Physiochemical Properties of Thin Film Composite Polyamide RO and NF Membranes. I. FTIR and XPS Characterization of Polyamide and Coating Layer Chemistry. *Desalination* **2009**, *242*, 149−167.

(37) Jiang, Z.; Karan, S.; Livingston, A. G. Water Transport through Ultrathin Polyamide Nanofilms Used for Reverse Osmosis. *Adv. Mater.* **2018**, *30*, No. 1705973.

(38) Coronell, O.; Mariñas, B. J.; Cahill, D. G. Depth Heterogeneity of Fully Aromatic Polyamide Active Layers in Reverse Osmosis and Nanofiltration Membranes. *Environ. Sci. Technol.* **2011**, *45*, 4513−4520.

(39) Dennison, J. M.; Xie, X.; Murphy, C. J.; Cahill, D. G. Density, Elastic Constants, and Thermal Conductivity of Interfacially Polymerized Polyamide Films for Reverse Osmosis Membranes. *ACS Appl. Nano Mater.* **2018**, *1*, 5008−5018.

(40) Nguyen, N.; Fargues, C.; Guiga, W.; Lameloise, M.-L. Assessing Nanofiltration and Reverse Osmosis for the Detoxification of Lignocellulosic Hydrolysates. *J. Membr. Sci.* **2015**, *487*, 40−50.

(41) Gerard, R.; Hachisuka, H.; Hirose, M. New Membrane Developments Expanding the Horizon for the Application of Reverse Osmosis Technology. *Desalination* **1998**, *119*, 47−55.

(42) Chen, Z.; Luo, J.; Hang, X.; Wan, Y. Physicochemical Characterization of Tight Nanofiltration Membranes for Dairy Wastewater Treatment. *J. Membr. Sci.* **2018**, *547*, 51−63.

(43) Sagne, C.; Fargues, C.; Broyart, B.; Lameloise, M. L.; Decloux, M. Modeling Permeation of Volatile Organic Molecules through Reverse Osmosis Spiral-Wound Membranes. *J. Membr. Sci.* **2009**, *330*, 40−50.

(44) Sagne, C.; Fargues, C.; Lewandowski, R.; Lameloise, M.-L.; Decloux, M. Screening of Reverse Osmosis Membranes for the Treatment and Reuse of Distillery Condensates into Alcoholic Fermentation. *Desalination* **2008**, *219*, 335−347.

(45) Freger, V. Swelling and Morphology of the Skin Layer of Polyamide Composite Membranes: An Atomic Force Microscopy Study. *Environ. Sci. Technol.* **2004**, *38*, 3168−3175.

(46) Cui, Y.; Liu, X.-Y.; Chung, T.-S. Ultrathin Polyamide Membranes Fabricated from Free-Standing Interfacial Polymerization: Synthesis, Modifications, and Post-Treatment. *Ind. Eng. Chem. Res.* **2017**, *56*, 513−523.

(47) Foglia, F.; Karan, S.; Nania, M.; Jiang, Z.; Porter, A. E.; Barker, R.; Livingston, A. G.; Cabral, J. T. Neutron Reflectivity and Performance of Polyamide Nanofilms for Water Desalination. *Adv. Funct. Mater.* **2017**, *27*, No. 1701738.

(48) Jin, Y.; Su, Z. Effects of Polymerization Conditions on Hydrophilic Groups in Aromatic Polyamide Thin Films. *J. Membr. Sci.* **2009**, *330*, 175−179.

(49) Dutta, D.; Bhattacharyya, A.; Ganguly, B. N. Microstructural Study of Aromatic Polyamide Membrane Material. *J. Membr. Sci.* **2003**, *224*, 127−135.

(50) Greenspan, L. Humidity Fixed Points of Binary Saturated Aqueous Solutions. *J. Res. Natl. Bur. Stand., Sect. A* **1977**, *81A*, 89−96.

(51) Kwak, S.-Y.; Ihm, D. W. Use of Atomic Force Microscopy and Solid-State NMR Spectroscopy to Characterize Structure-Property-Performance Correlation in High-Flux Reverse Osmosis (RO) Membranes. *J. Membr. Sci.* **1999**, *158*, 143−153.

(52) Pacheco, F. A.; Pinnau, I.; Reinhard, M.; Leckie, J. O. Characterization of Isolated Polyamide Thin Films of RO and NF Membranes Using Novel TEM Techniques. *J. Membr. Sci.* **2010**, *358*, 51−59.

(53) Li, Q.; Pan, X.; Hou, C.; Jin, Y.; Dai, H.; Wang, H.; Zhao, X.; Liu, X. Exploring the Dependence of Bulk Properties on Surface Chemistries and Microstructures of Commercially Composite RO Membranes by Novel Characterization Approaches. *Desalination* **2012**, *292*, 9−18.

(54) Nowbahar, A.; Mansard, V.; Mecca, J. M.; Paul, M.; Arrowood, T.; Squires, T. M. Measuring Interfacial Polymerization Kinetics Using Microfluidic Interferometry. *J. Am. Chem. Soc.* **2018**, *140*, 3173−3176.

(55) Dražević, E.; Košutić, K.; Freger, V. Permeability and Selectivity of Reverse Osmosis Membranes: Correlation to Swelling Revisited. *Water Res.* **2014**, *49*, 444−452.

(56) Zhang, X.; Cahill, D. G.; Coronell, O.; Mariñas, B. J. Absorption of Water in the Active Layer of Reverse Osmosis Membranes. *J. Membr. Sci.* **2009**, *331*, 143−151.

(57) Van Krevelen, D. W.; Te Nijenhuis, K. Optical Properties. *Properties of Polymers: Their Correlation with Chemical Structure; Their Numerical Estimation and Prediction from Additive Group Contributions*, 4th ed.; Elsevier: Amsterdam, The Netherlands, 2009; pp 290−296.

(58) Ben-David, A.; Oren, Y.; Freger, V. Thermodynamic Factors in Partitioning and Rejection of Organic Compounds by Polyamide Composite Membranes. *Environ. Sci. Technol.* **2006**, *40*, 7023−7028.

(59) Kolev, V.; Freger, V. Hydration, Porosity and Water Dynamics in the Polyamide Layer of Reverse Osmosis Membranes: A Molecular Dynamics Study. *Polymer* **2014**, *55*, 1420−1426.

(60) Shen, M.; Keten, S.; Lueptow, R. M. Rejection Mechanisms for Contaminants in Polyamide Reverse Osmosis Membranes. *J. Membr. Sci.* **2016**, *509*, 36−47.

(61) Akin, O.; Temelli, F. Probing the Hydrophobicity of Commercial Reverse Osmosis Membranes Produced by Interfacial Polymerization Using Contact Angle, XPS, FTIR, FE-SEM and AFM. *Desalination* **2011**, *278*, 387−396.

(62) Kim, S. H.; Kwak, S.-Y.; Suzuki, T. Positron Annihilation Spectroscopic Evidence to Demonstrate the Flux-Enhancement Mechanism in Morphology-Controlled Thin-Film-Composite (TFC) Membrane. *Environ. Sci. Technol.* **2005**, *39*, 1764−1770.

(63) Morgan, P. W.; Kwolek, S. L. Interfacial Polycondensation. II. Fundamentals of Polymer Formation at Liquid Interfaces. *J. Polym. Sci.* **1959**, *40*, 299−327.

(64) Freger, V.; Srebnik, S. Mathematical Model of Charge and Density Distributions in Interfacial Polymerization of Thin Films. *J. Appl. Polym. Sci.* **2003**, *88*, 1162−1169.